The Role of Fluorine in F-La/TiO₂ Photocatalysts on Photocatalytic Decomposition of Methanol-Water Solution

Miroslava Edelmannová [1,2], Lada Dubnová [3], Martin Reli [1] , Vendula Meinhardová [3], Pengwei Huo [4], Urška Lavrenčič Štangar [5], Libor Čapek [3] and Kamila Kočí [1,*]

[1] Institute of Environmental Technology, VŠB-Technical University of Ostrava, 17. listopadu 15/2172, 70800 Ostrava, Czech Republic
[2] Faculty of Materials Science and Technology, VŠB-Technical University of Ostrava, 17. listopadu 15/2172, 70800 Ostrava, Czech Republic
[3] Faculty of Chemical Technology, University of Pardubice, Studentská 573, 53210 Pardubice, Czech Republic
[4] School of Chemistry and Chemical Engineering, Jiangsu University, 301 Xuefu Road, Zhenjiang 212013, China
[5] Faculty of Chemistry and Chemical Technology, University of Ljubljana, Večna pot 113, P.O Box 537, 1001 Ljubljana, Slovenia
* Correspondence: kamila.koci@vsb.cz

check for updates

Abstract: F-La/TiO₂ photocatalysts were studied in photocatalytic decomposition water-methanol solution. The structural, textural, optical, and electronic properties of F-La/TiO₂ photocatalysts were studied by combination of X-ray powder diffraction (XRD), nitrogen physisorption, Ultraviolet–visible diffuse reflectance spectroscopy (UV-Vis DRS), Electrochemical impedance spectroscopy (EIS), and X-ray fluorescence (XPS). The production of hydrogen in the presence of 2.8F-La/TiO₂ was nearly up to 3 times higher than in the presence of pure TiO₂. The photocatalytic performance of F-La/TiO₂ increased with increasing photocurrent response and conductivity originating from the higher amount of fluorine presented in the lattice of TiO₂.

Keywords: hydrogen production; fluorine; lanthanum; titanium dioxide

1. Introduction

Lately, hydrogen has acquired significant attention as a next-generation energy carrier. Photocatalytic water splitting into hydrogen and oxygen in the presence of semiconductor photocatalysts is an attractive process of how to produce it. There are many reviews focusing on this topic every year, e.g., [1–3]. Higher efficiency of hydrogen production has been achieved in photocatalytic water splitting under presence of sacrificial agent, among others, preventing the recombination of electron-hole pairs [1].

Since the discovery of water splitting on TiO₂ electrodes in the presence of UV irradiation, TiO₂-based photocatalytic materials have received much attention as a photocatalytic semiconductor. The advantages of TiO₂-based materials include their biological and chemical inertness, stability, and low cost. On the other hand, pristine TiO₂ photocatalysts are limited by the fast rate of recombination of photogenerated electron-hole pairs and by their wide band gap, which requires UV irradiation for activation. For these reasons, the modification of TiO₂ is required [4–6].

There are different strategies to prepare modified TiO₂, involving diverse metal or non-metal doping [7–9], multi-phase composition, or combination of TiO₂ with other semiconductors [10,11]. The presence of surface defects and especially the oxygen vacancies present in TiO₂ crystalline structure

are among the most important factors determining the resulting photocatalytic behavior [12,13]. From this point of view, co-doping by both metal and non-metal atoms is a promising direction of TiO_2 modification [14].

Fluorine doped TiO_2 photocatalyst can induce visible-light-driven photocatalysis due to the formation of oxygen vacancies. $F-TiO_2$-based photocatalysts have been studied in many reactions, for example, in oxidation of 2-propanol [15] and degradation of dyes [16]. The photocatalytic behavior of $F-TiO_2$ photocatalysts has been explained by the positive role of fluoride ions to morphology [17], the presence of surface defects forming surface O- species [13], oxygen vacancies [16,18], and higher conductivity [15]. Nevertheless, the role of fluorine on the photocatalytic behaviour of $F-TiO_2$-based materials is still under discussion. The problem is partially due to the presence of residual fluoride (after synthesis) adsorbed on the surface of TiO_2. Surface fluorine has been removed by NaOH which led to the improvement of photocatalytic behavior [13].

This article is a natural continuation of our previous research focused on La/TiO_2 [19] and $N-La/TiO_2$ [20] photocatalysts. The role of lanthanum in La/TiO_2 to its photocatalytic behaviors was reported [19]. Subsequently, the optimal amount of La (ca. 0.2 wt %) was used and the critical parameters of $N-La/TiO_2$ playing a role in the decomposition of methanol-water solution [20] were specified. In the current study, a simple method to synthesize TiO_2 photocatalysts doped with non-metal (fluorine) and metal (lanthanum) elements is used [21]. The physico-chemical properties of $F-La/TiO_2$ photocatalysts were characterized by XRD, nitrogen physisorption, UV-Vis, EIS, and XPS. The photocatalytic performance of $F-La/TiO_2$ photocatalysts was investigated in the decomposition of methanol-water solution. The attention was focused on the explanation of the contribution of fluorine to the photocatalytic behavior of $F-La/TiO_2$ photocatalysts.

2. Materials and Methods

2.1. Preparation of Materials

Basic powder materials TiO_2 and 0.2 wt % La/TiO_2, were prepared by the sol-gel method within the environment of reverse micelles (Triton X-114 in cyclohexane). Solution containing Triton X-114 (laboratory grade, Sigma Aldrich, Saint Louis, MO, USA), cyclohexane (≥99.5%, Fluka Chemika, Munich, Germany), deionized water with lanthanum (III) nitrate hexahydrate ($La(NO_3)_3 \cdot 6H_2O$, 99.99%, Sigma Aldrich, Saint Louis, MO, USA) dissolved in ethanol was stirred for 20 min. Thereafter, titanium (IV) propoxide (98%, Sigma Aldrich, Saint Louis, MO, USA) was added to this solution and mixed again for 20 min. The resulting sols were poured into Petri dishes and left for 24 h at laboratory temperature. The final dry material after gelation was transferred into ceramic crucibles and calcined at 450 °C for 4 h (without heating rate).

TiO_2 or La/TiO_2 powder was added to KBF_4 (96%, Sigma Aldrich, Saint Louis, MO, USA), which was in 0.05 M 100 mL nitric acid (HNO_3, 65%, Fluka Chemika, Munich, Germany), the suspension was stirred for 2 h at laboratory temperature and then the mixture was maintained at 180 °C for 24 h. After hydrothermal reaction, the precipitates were filtered, washed by 500 mL deionized water (to get pH = 7) and dried to obtain $F-La/TiO_2$ hydrothermal product.

2.2. Characterization of Materials

Textural, structural, optical, and electronic properties of all photocatalysts were characterized in detail by nitrogen physisorption [22,23], powder X-ray diffraction (XRD) [22,23], X-ray fluorescence (XRF) [20], diffuse reflectance UV-vis spectroscopy (DRS UV-Vis) [22,24], X-ray photoelectron spectroscopy (XPS) [22], and photoelectrochemical measurements [23] (see Supplementary Materials). Chemical components and the binding energies of CdS/CN were analyzed by XPS (Thermo Scientific ESCALAB 250Xi A1440 system, Waltham, MA, USA). Electrochemical impedance spectroscopy (EIS) analysis was measured by using a CHI 760E electrochemical workstation.

2.3. Photocatalytic Test

The photocatalytic decomposition of the methanol-water solution was carried out in a batch photoreactor with a 8 W Hg lamp (λ = 365 nm, see Supplementary Materials) [22].

3. Results and Discussion

3.1. Structural and Optical Properties of La/and F-La/TiO$_2$

Table 1 gives the content of La in La/TiO$_2$ and F-La/TiO$_2$ photocatalysts determined by XRF. The F-La/TiO$_2$ photocatalysts contained the real amount of La close to its theoretical amount (0.20 wt % La). La/TiO$_2$ contained slightly lower concentration of La in contrast to the theoretical one that could be caused by very low amount of La precursors used in the synthesis. The textural parameters of studied materials are also shown in Table 1. All TiO$_2$, La/TiO$_2$ and F-La/TiO$_2$ photocatalysts possessed similar specific surface area values, close to 80 m^2 g^{-1}.

Table 1. Composition, textural, and optical properties of investigated photocatalysts.

Photocatalyst	XRF	Textural Properties	DRS UV-vis
	The Content of La (wt %)	**S$_{BET}$ (m^2.g^{-1})**	**Indirect Band Gap (eV)**
TiO$_2$	-	80	2.85
La/TiO$_2$	0.13	73	2.95
2.8F-La/TiO$_2$	0.20	84	3.01
4.1F-La/TiO$_2$	0.22	79	3.00

Figure 1 shows the X-ray patterns of the TiO$_2$, La/ and F-La/TiO$_2$ photocatalysts. Diffractograms of all photocatalysts showed diffraction lines characteristic of tetragonal modification of anatase (ICDD card no. 00-021-1272; space group I4$_1$/amd, lattice constants $a = b = 0.37852$ nm and $c = 0.95139$ nm). Coherent domain sizes were in the range of 12.9 and 14.4 nm (Table 2). Any additional diffraction lines reflecting the presence of rutile phase, brookite phase, or lanthanum related phase (pure or oxidic form) were not observed. All materials exhibited approximately the same values of lattice parameters a and c (Table 2).
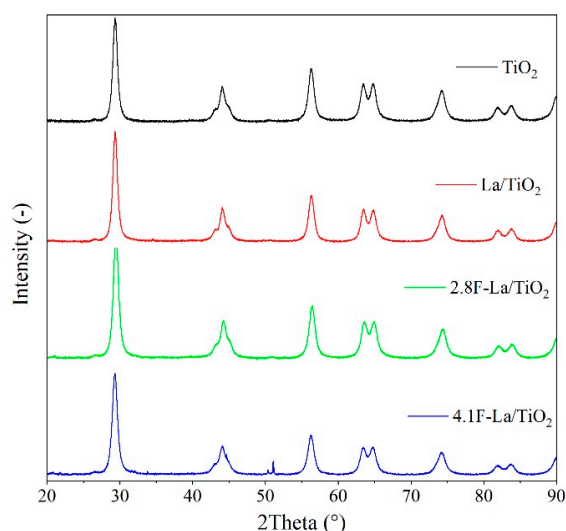

Figure 1. XRD patterns of investigated photocatalysts.

Table 2. Structural and microstructural properties of investigated photocatalysts.

Photocatalyst	Anatase Crystallite Size nm	Lattice Parameters	
		a nm	*c* nm
TiO_2	14.4	0.3788	0.9510
La/TiO_2	14.7	0.3787	0.9504
$2.8F-La/TiO_2$	13.3	0.3787	0.9506
$4.1F-La/TiO_2$	12.9	0.3788	0.9505

The values of the indirect band gap energies of TiO_2, La/TiO_2, and $F-La/TiO_2$, presented in Table 1, were determined from the dependencies of $(\alpha \cdot h \cdot \nu)^{1/2}$ on energy (Figure 2). The band gap energies of the TiO_2, La/TiO_2 and $F-La/TiO_2$ photocatalysts had the values in the range of 2.85 to 3.01 eV, with TiO_2 being the lowest band gap energy value. Nevertheless, the mentioned difference is marginal. Thus, the addition of fluorine did not lead to the change of band gap energies.
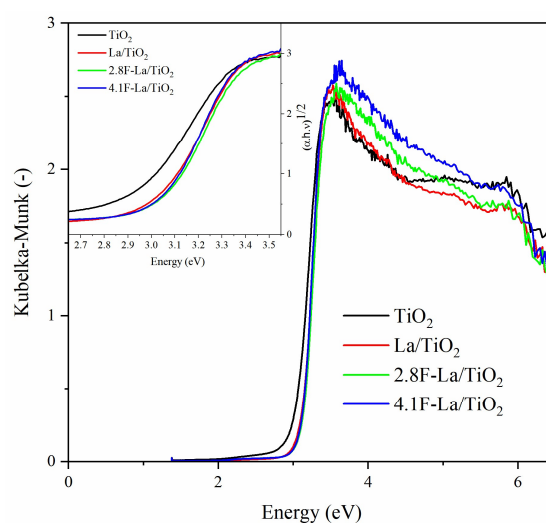

Figure 2. UV-Vis DRS spectra of investigated photocatalysts. The cut-out contains the Tauc plot and the determination of the indirect band gap energy values.

XPS analysis identified five different elements (Ti, O, C, La, and F) presented on the surface of investigated photocatalysts (Figure 3 and Table 3). The Figure 3a shows the O 1s spectrum of the materials. There are two binding energy peaks at about 529.7 eV and 531.3 eV in all materials, which corresponds to the Ti-O and O–H bonds [25]. With the introduction of F element, a new peak of binding energy appears at about 533.3 eV which corresponds to the H_2O molecules adsorbed on the surface of the photocatalyst [26], and the intensity of this peak increases with the increase of the amount of F. This phenomenon proves that the doping of F element greatly improves the hydrophilicity of samples [27], which is beneficial for the photocatalytic process. The XPS spectrum of Ti 2p shows two typical binding energy peaks at about 458.6 eV and 464.4 eV due to the Ti $2p_{3/2}$ and Ti $2p_{1/2}$ corresponding to +4 valence state of Ti and showing that the elements of Ti firstly existed as Ti^{4+} in the material (Figure 3b) [28]. The doublet peaks derived from spin-orbit splitting of Ti2p affirmed the difference in binding energy is around 5.8 eV. This results also confirm that TiO_2 phase in the photocatalysts exists only in the presence of anatase, which is the agreement with the XRD analysis. The XPS spectrum in Figure 3c confirms that the La element was successfully doped into La/TiO_2, $2.8F-La/TiO_2$, and $4.1F-La/TiO_2$ photocatalysts, corresponding to the binding energy peaks of 836.8 and 854.7 eV in the La $3d_{5/2}$ and La $3d_{3/2}$, respectively [29]. However, its intensity is marginal and the surface atomic concentration of La is limiting to zero. It is in agreement with our previous works [19], where we also did not observe measurable concentration of La on the surface of $La-TiO_2$ materials with low La content. Figure 3d displays the XPS spectrum of F elements of $2.8F-La/TiO_2$ and $4.1F-La/TiO_2$.

The binding energy peak appeared at about 684.0 eV and is caused by the F elements adsorbed on the surface of the material (i.e., surface fluorination; T–F bond forming by substitution of OH– group), and the other peak appeared at about 689.0 eV which is caused by F element incorporated into the lattice of TiO_2 [30]. Fluorine present in the lattice of TiO_2 results in the formation of Ti^{3+} sites [31]. In order to further analyze the doping of F element in different samples, we conducted integral calculation of the content of F element in these two different forms through Gaussian fitting and the specific results are displayed in Table 4. Due to the fact, that the atom radius of fluorine is resembling oxygen, the substitute of the oxygen atoms joined Ti atoms in the TiO_2 lattice by atoms of fluorine, which is relatively facile [28]. According to the XPS analysis, the total content of F in the 2.8F-La/TiO_2 and 4.1F-La/TiO_2 photocatalysts was determined to be at 2.82% and 4.13%, respectively.
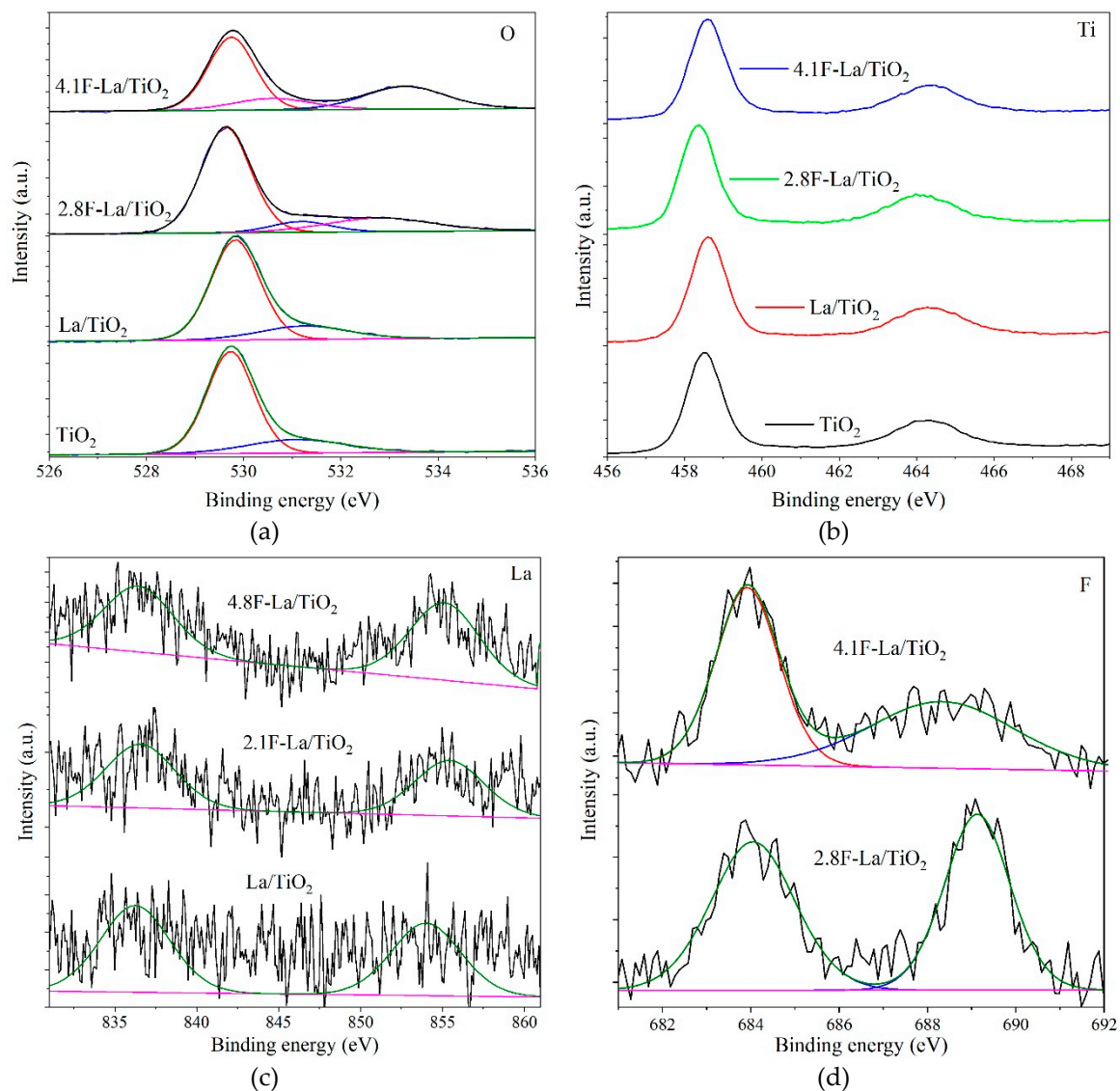

Figure 3. XPS spectra for oxygen (**a**), titanium (**b**), lanthanum (**c**) and fluorine (**d**) of investigated photocatalysts.

Table 3. Surface concentration of Ti, O, F, and C elements determined by XPS.

Photocatalyst	Ti (at %)	O (at %)	F (at %)	C (at %)	O/Ti
TiO_2	31.27	60.44	0	8.30	1.93
La/TiO_2	30.84	59.58	0	9.58	1.93
2.8F-La/TiO_2	26.26	49.46	2.83	21.45	1.88
4.1F-La/TiO_2	30.63	58.31	4.14	6.93	1.90

Table 4. Surface concentration of surface fluorine and lattice fluorine determined by XPS.

Photocatalyst	Content of F (at %)	Surface Fluorine (at %)	Lattice Fluorine (at %)	Ratio of Lattice and Surface Fluorine
2.8F-La/TiO$_2$	2.83	1.47	1.36	0.931
4.1F-La/TiO$_2$	4.14	2.22	1.92	0.865

Figure 4 shows the photocurrent response for the studied photocatalysts. Photocurrent generation can predict behavior of the photocatalyst after irradiation but does not supplement its photocatalytic activity. Since the photocurrent is measured under applied external potential of 1 V, most of the generated electrons are forced to migrate to the ITO foil and measured as current. Simply said, external potential is strongly suppressing the recombination of charge carriers. Based on the results, we can claim 2.8F-La/TiO$_2$ photocatalyst generates the highest amount of charge carriers after irradiation with 365 nm. The reason for lower photocurrent values in this study compared to that reported for La-based materials in our works [19,20] is due to the different slits setting. There are two slits, one in front of the monochromator and the second behind the monochromator, which can be set to different values. While previous measurements were done with completely opened slits, the slit behind the monochromator was currently set to 1 mm in order to have more precise wavelength steps. From that reason, the comparison is not possible.
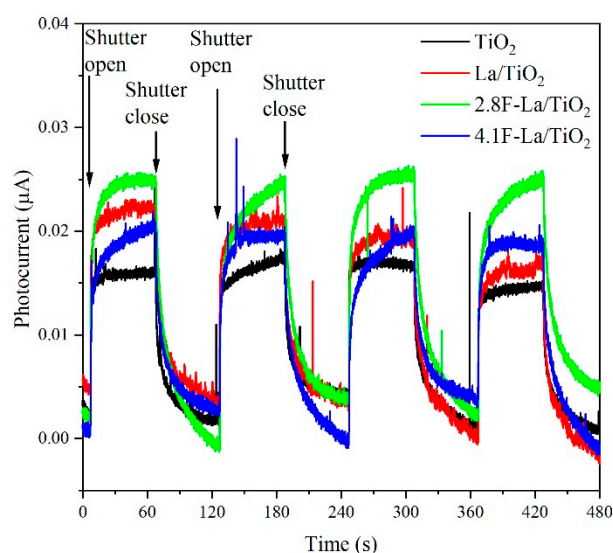
Figure 4. Photocurrent responses of prepared photocatalysts under applied external potential 1 V and irradiated under 365 nm.

The electrochemical impedance spectroscopy (EIS) technique has been used to research the electron transfer efficiency of the prepared materials (Figure 5). The semicircle in the EIS spectra is caused by contribution from the constant phase element at the photocatalyst/electrolyte interface and the charge transfer resistance. The small semicircle radius of the material indicates a smaller impedance in the photogenerated electron transfer process [32–34]. The arc radii of TiO$_2$ is shown as the black point plot in Figure 5. And it is clear that the doping of the La element caused the impedance of the sample to be lower than that of the pure TiO$_2$. Subsequent increase of conductivity (decrease of semicircle radius) was observed for F-La/TiO$_2$ photocatalysts. 2.8F-La/TiO$_2$ with the highest conductivity (EIS) also exhibited the highest photocurrent density. After that, the conductivity of photocatalysts decreased with the same order as in the case of the photocurrent response.
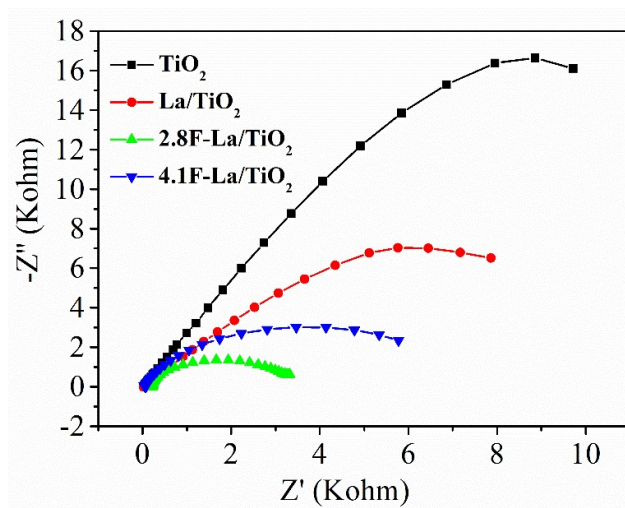
Figure 5. Electron transfer efficiency of investigated photocatalysts.

The small fluorine doping concentration (2.8F-La/TiO$_2$) caused that the F doped in TiO$_2$ favors the transfer of the electrons and represses the recombination of charge in TiO$_2$ [35–37]. It can be due to the fact that the Ti^{3+} surface states and the oxygen vacancies could capture photoelectrons and transfer them to O$_2$ adsorbed on the surface of TiO$_2$ [38,39]. In the case of 4.1F-La/TiO$_2$, both the concentration of fluorine and the semicircle were higher. The fluorine doping can act as a center of recombination, which increases the charge recombination in TiO$_2$ because the average distance between two trap sites goes down with the growing dopants number [35,38,40].

3.2. Photocatalytic Activity of La/and F-La/TiO$_2$

The photocatalytic generation of hydrogen from methanol-water solution during UVA illumination in the presence of investigated photocatalysts is shown in Figure 6. The formation of hydrogen is decreasing in order: 2.8F-La/TiO$_2$ > 4.1F-La/TiO$_2$ ≈ La/TiO$_2$ > TiO$_2$. The production of hydrogen in the presence of 2.8F-La/TiO$_2$ was nearly up to 3 times higher than in the presence of pure TiO$_2$. It also should be stressed that the hydrogen yield formed over 2.8F-La/TiO$_2$ (Figure 6) is higher than for N-La/TiO$_2$ [20].
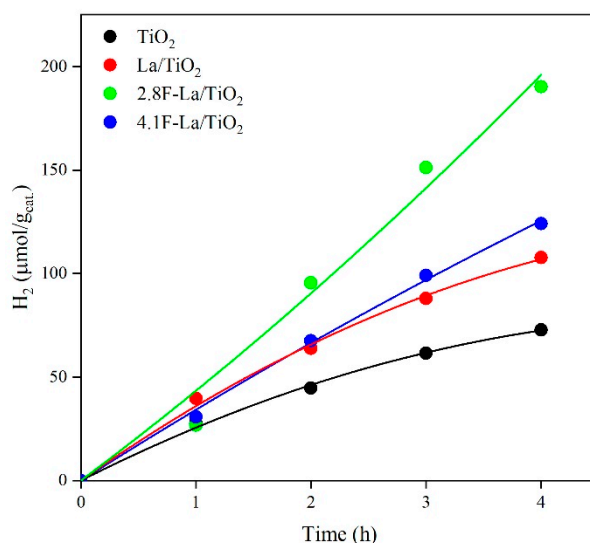

Figure 6. Generation of hydrogen in the photocatalytic degradation of methanol-water solution in the presence of the investigated photocatalysts.

3.3. Properties of F-La/TiO₂ Playing the Role in Photacatalytic Reaction

In general, the photocatalytic activity of F-La/TiO$_2$ photocatalysts can be influenced by several factors, such as (i) band gap energy, (ii) specific surface area, (iii) rate of the recombination of electron-hole pairs, (iv) presence of oxygen vacancies, (v) amount of lattice and surface O species, and (vi) phase composition. In our case, F-La/TiO$_2$ photocatalysts and pure TiO$_2$ exhibited approximately the same structure, specific surface area (Table 1), and band gap energy (Table 1 and Figure 2).

The hydrogen yield (Figure 6) clearly increased with increasing photocurrent response (Figure 4) and increasing conductivity (Figure 5). The increasing value of both photocurrent and conductivity can reflect a decrease of the recombination probability of photogenerated electron-hole pairs. Figure 7 shows the correlation between the amount of hydrogen and the photocurrent response. The trend of photocatalytic activity of F-La/TiO$_2$ corresponds to their photocurrent responses (Figure 7b). Low photocurrent means lower amount of generated electron-hole pair after irradiation. The 2.8F-La/TiO$_2$ photocatalyst showed both the highest photocatalytic activity and the photocurrent response as well. This is in agreement with many other authors [19,41–43].
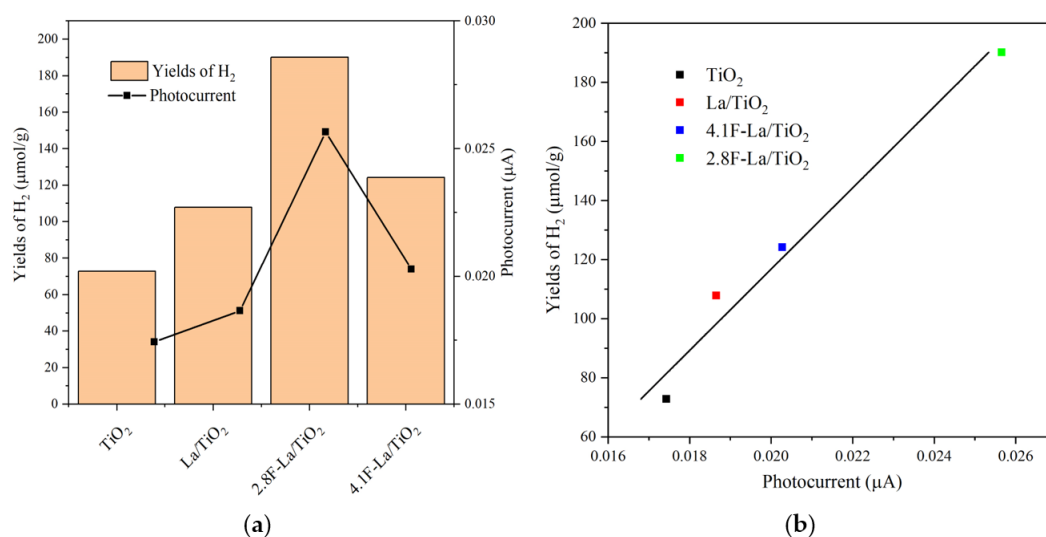

(a)　　　　　　　　　　　　　　　(b)

Figure 7. Correlation between the photocatalytic activity in the photocatalytic decomposition of methanol-water solution (**a**) and the hydrogen yields dependence on photocurrent (**b**) in the presence of the investigated photocatalysts and current generation. Current responses were obtained at 365 nm under external potential of 1.0 V.

The value of photocurrent response and conductivity can reflect the combination of two factors, i.e., the amount of fluorine substituted into the oxygen sites of the TiO$_2$ lattice and the amount of surface O-sites.

Combining with the XPS results (Figure 3d), it was affirmed that atoms of fluorine was substituted also into the oxygen sites of the TiO$_2$ lattice. The charge imbalance is formed when -1 F ions replaced the -2 oxygen sites. The excess positive charge is possible to be neutralized by creating hydroxide ions which form from surface adsorbed hydroxyl groups. Consequence to this, more reactive oxygen species as hydroxyl radicals and superoxide free radicals can be created, which show the existence of oxygen vacancies. These oxygen species have strong oxidative capability and play a significant role in the photocatalytic degradation of methanol-water solution [18,44]. In agreement with that, 2.8F-La/TiO$_2$ possessed a higher ratio of lattice to surface fluorine species (Table 4) and higher hydrogen yield (Figure 7), as well as the highest photocurrent density and conductivity (EIS).

Previously, we observed for La-N/TiO$_2$-based photocatalysts that the hydrogen yield increased with increasing amount of oxygen vacancies and decreasing amount of surface oxygen species (surface lattice O species and hydroxyl groups, XPS) [20]. In principle, the amount of produced hydrogen yield

(Figure 7) increased with decreasing content of surface O-sites also for La-F/TiO$_2$ (Table 3), but the clear correlation could not be done due to the different population of surface C-species among the individual materials. Thus, we calculated O/Ti surface atomic ratio (Table 3), with the lowest value for 2.8F-La/TiO$_2$. The O/Ti surface atomic ratio was lower for both F-La/TiO$_2$ photocatalysts than for TiO$_2$ and La/TiO$_2$ which show to decrease the amount of surface oxygen species after F-loading.

4. Conclusions

Based on the above characterizations and photocatalytic activity, co-doping by lanthanum and fluorine proved to be an effective method to prepare the highly photoactive TiO$_2$-based photocatalysts for production of hydrogen from photocatalytic decomposition of methanol-water solution.

The anatase TiO$_2$ photocatalysts with different F amounts and the similar La amount (0.13–0.21 wt %) were prepared by sol-gel method and in detail characterized by various methods. The highest hydrogen yield during the photocatalytic decomposition of methanol-water solution exhibited the 2.8 F-La/TiO$_2$ photocatalyst.

The prepared F-La/TiO$_2$ (3.36 and 4.45 at % fluorine content) photocatalyst showed enhanced photocatalytic activity in decomposition of methanol-water solution under 365 nm illumination, the hydrogen production in the presence of 2.8F-La/TiO$_2$ and 4.1F-La/TiO$_2$ photocatalysts was nearly up to 3 and 2 times higher in comparison to the pure TiO$_2$, respectively. The photocatalytic performance of F-La/TiO$_2$ increased with increasing photocurrent response and conductivity. These results indicated that the fluorine ions were successfully incorporated into the lattice of TiO$_2$. Moreover, the luorine and lanthanum co-doping of TiO$_2$ photocatalyst can effectively decrease the recombination probability of photogenerated electron-hole pairs.

References

1. Fajrina, N.; Tahir, M. A critical review in strategies to improve photocatalytic water splitting towards hydrogen production. *Int. J. Hydrogen Energy* **2019**, *44*, 540–577. [CrossRef]
2. Kumaravel, V.; Mathew, S.; Bartlett, J.; Pillai, S.C. Photocatalytic hydrogen production using metal doped TiO$_2$: A review of recent advances. *Appl. Catal. B* **2019**, *244*, 1021–1064. [CrossRef]
3. Wang, Z.; Li, C.; Domen, K. Recent developments in heterogeneous photocatalysts for solar-driven overall water splitting. *Chem. Soc. Rev.* **2019**, *48*, 2109–2125. [CrossRef] [PubMed]
4. Fang, W.; Xing, M.; Zhang, J. Modifications on reduced titanium dioxide photocatalysts: A review. *J. Photochem. Photobiol. C* **2017**, *32*, 21–39. [CrossRef]
5. Ma, Y.; Wang, X.; Jia, Y.; Chen, X.; Han, H.; Li, C. Titanium dioxide-based nanomaterials for photocatalytic fuel generations. *Chem. Rev.* **2014**, *114*, 9987–10043. [CrossRef] [PubMed]
6. Low, J.; Cheng, B.; Yu, J. Surface modification and enhanced photocatalytic CO$_2$ reduction performance of TiO$_2$: A review. *Appl. Surf. Sci.* **2017**, *392*, 658–686. [CrossRef]
7. Gomes, J.; Lincho, J.; Domingues, E.; Quinta-Ferreira, M.R.; Martins, C.R. N–TiO$_2$ Photocatalysts: A Review of Their Characteristics and Capacity for Emerging Contaminants Removal. *Water* **2019**, *11*, 373. [CrossRef]

8. Devaiah, D.; Jampaiah, D.; Saikia, P.; Reddy, B.M. Structure dependent catalytic activity of $Ce_{0.8}Tb_{0.2}O_{2-\delta}$ and TiO_2 supported $Ce_{0.8}Tb_{0.2}O_{2-\delta}$ solid solutions for CO oxidation. *J. Ind. Eng. Chem.* **2014**, *20*, 444–453. [CrossRef]

9. Smirniotis, P.G.; Boningari, T.; Damma, D.; Inturi, S.N.R. Single-step rapid aerosol synthesis of N-doped TiO_2 for enhanced visible light photocatalytic activity. *Catal. Commun.* **2018**, *113*, 1–5. [CrossRef]

10. Low, J.; Yu, J.; Jaroniec, M.; Wageh, S.; Al-Ghamdi, A.A. Heterojunction Photocatalysts. *Adv. Mater.* **2017**, *29*, 1601694. [CrossRef]

11. Wei, L.; Yu, C.; Zhang, Q.; Liu, H.; Wang, Y. TiO_2-based heterojunction photocatalysts for photocatalytic reduction of CO_2 into solar fuels. *J. Mater. Chem. A* **2018**, *6*, 22411–22436. [CrossRef]

12. Kubacka, A.; Fernández-García, M.; Colón, G. Advanced Nanoarchitectures for Solar Photocatalytic Applications. *Chem. Rev.* **2012**, *112*, 1555–1614. [CrossRef] [PubMed]

13. Yu, X.; Jeon, B.; Kim, Y.K. Dominant Influence of the Surface on the Photoactivity of Shape-Controlled Anatase TiO_2 Nanocrystals. *ACS Catal.* **2015**, *5*, 3316–3322. [CrossRef]

14. Pan, X.; Yang, M.-Q.; Fu, X.; Zhang, N.; Xu, Y.-J. Defective TiO_2 with oxygen vacancies: Synthesis, properties and photocatalytic applications. *Nanoscale* **2013**, *5*, 3601–3614. [CrossRef] [PubMed]

15. Bellardita, M.; Garlisi, C.; Venezia, A.M.; Palmisano, G.; Palmisano, L. Influence of fluorine on the synthesis of anatase TiO_2 for photocatalytic partial oxidation: Are exposed facets the main actors? *Catal. Sci. Technol.* **2018**, *8*, 1606–1620. [CrossRef]

16. Du, M.; Qiu, B.; Zhu, Q.; Xing, M.; Zhang, J. Fluorine doped TiO_2/mesocellular foams with an efficient photocatalytic activity. *Catal. Today* **2019**, *327*, 340–346. [CrossRef]

17. Pan, J.; Liu, G.; Lu, G.Q.; Cheng, H.-M. On the True Photoreactivity Order of {001}, {010}, and {101} Facets of Anatase TiO_2 Crystals. *Angew. Chem. Int. Ed.* **2011**, *50*, 2133–2137. [CrossRef]

18. Li, C.; Sun, Z.; Ma, R.; Xue, Y.; Zheng, S. Fluorine doped anatase TiO_2 with exposed reactive (001) facets supported on porous diatomite for enhanced visible-light photocatalytic activity. *Microporous Mesoporous Mater.* **2017**, *243*, 281–290. [CrossRef]

19. Kočí, K.; Troppová, I.; Edelmannová, M.; Starostka, J.; Matějová, L.; Lang, J.; Reli, M.; Drobná, H.; Rokicińska, A.; Kuśtrowski, P.; et al. Photocatalytic decomposition of methanol over La/TiO_2 materials. *Environ. Sci. Pollut. Res. Int.* **2018**, *25*, 34818–34825. [CrossRef]

20. Dubnová, L.; Zvolská, M.; Edelmannová, M.; Matějová, L.; Reli, M.; Drobná, H.; Kuśtrowski, P.; Kočí, K.; Čapek, L. Photocatalytic decomposition of methanol-water solution over N-La/TiO_2 photocatalysts. *Appl. Surf. Sci.* **2019**, *469*, 879–886. [CrossRef]

21. Wu, Y.; Zhou, Z.; Wang, W.; Huang, Y.; Shen, S. A novel and facile method to synthesize crystalline-disordered core–shell anatase (La, F)–TiO_2. *Mater. Lett.* **2013**, *98*, 261–264. [CrossRef]

22. Koci, K.; Troppova, I.; Reli, M.; Matejova, L.; Edelmannova, M.; Drobna, H.; Dubnova, L.; Rokicinska, A.; Kustrowski, P.; Capek, L. Nd/TiO_2 Anatase-Brookite Photocatalysts for Photocatalytic Decomposition of Methanol. *Front. Chem.* **2018**, *6*, 44. [CrossRef] [PubMed]

23. Kočí, K.; Reli, M.; Edelmannová, M.; Troppová, I.; Drobná, H.; Rokicińska, A.; Kuśtrowski, P.; Dvoranová, D.; Čapek, L. Photocatalytic hydrogen production from methanol over Nd/TiO_2. *J. Photochem. Photobiol. A* **2018**. [CrossRef]

24. Reli, M.; Ambrozova, N.; Sihor, M.; Matejova, L.; Capek, L.; Obalova, L.; Matej, Z.; Kotarba, A.; Koci, K. Novel cerium doped titania catalysts for photocatalytic decomposition of ammonia. *Appl. Catal. B* **2015**, *178*, 108–116. [CrossRef]

25. Wang, H.; Wu, D.; Liu, C.; Guan, J.; Li, J.; Huo, P.; Liu, X.; Wang, Q.; Yan, Y. Fabrication of Ag/In_2O_3/TiO_2/HNTs hybrid-structured and plasma effect photocatalysts for enhanced charges transfer and photocatalytic activity. *J. Ind. Eng. Chem.* **2018**, *67*, 164–174. [CrossRef]

26. Gao, Q.; Si, F.; Zhang, S.; Fang, Y.; Chen, X.; Yang, S. Hydrogenated F-doped TiO_2 for photocatalytic hydrogen evolution and pollutant degradation. *Int. J. Hydrogen Energy* **2019**, *44*, 8011–8019. [CrossRef]

27. Tang, J.; Quan, H.; Ye, J. Photocatalytic Properties and Photoinduced Hydrophilicity of Surface-Fluorinated TiO_2. *Chem. Mater.* **2007**, *19*, 116–122. [CrossRef]

28. Li, H.; Gao, Y.; Wu, X.; Lee, P.-H.; Shih, K. Fabrication of Heterostructured g-C_3N_4/Ag-TiO_2 Hybrid Photocatalyst with Enhanced Performance in Photocatalytic Conversion of CO_2 Under Simulated Sunlight Irradiation. *Appl. Surf. Sci.* **2017**, *402*, 198–207. [CrossRef]

29.　Huo, Y.; Zhu, J.; Li, J.; Li, G.; Li, H. An active La/TiO$_2$ photocatalyst prepared by ultrasonication-assisted sol–gel method followed by treatment under supercritical conditions. *J. Mol. Catal. A Chem.* **2007**, *278*, 237–243. [CrossRef]

30.　Fu, W.; Ding, S.; Wang, Y.; Wu, L.; Zhang, D.; Pan, Z.; Wang, R.; Zhang, Z.; Qiu, S. F, Ca co-doped TiO$_2$ nanocrystals with enhanced photocatalytic activity. *Dalton Trans.* **2014**, *43*, 16160–16163. [CrossRef]

31.　Czoska, A.M.; Livraghi, S.; Chiesa, M.; Giamello, E.; Agnoli, S.; Granozzi, G.; Finazzi, E.; Valentin, C.D.; Pacchioni, G. The Nature of Defects in Fluorine-Doped TiO$_2$. *J. Phys. Chem. C* **2008**, *112*, 8951–8956. [CrossRef]

32.　Li, X.; Liu, C.; Wu, D.; Li, J.; Huo, P.; Wang, H. Improved charge transfer by size-dependent plasmonic Au on C$_3$N$_4$ for efficient photocatalytic oxidation of RhB and CO$_2$ reduction. *Chin. J. Catal.* **2019**, *40*, 928–939. [CrossRef]

33.　Zhou, Y.; Li, J.; Liu, C.; Huo, P.; Wang, H. Construction of 3D porous g-C$_3$N$_4$/AgBr/rGO composite for excellent visible light photocatalytic activity. *Appl. Surf. Sci.* **2018**, *458*, 586–596. [CrossRef]

34.　Liu, C.; Li, J.; Sun, L.; Zhou, Y.; Liu, C.; Wang, H.; Huo, P.; Ma, C.; Yan, Y. Visible-light driven photocatalyst of CdTe/CdS homologous heterojunction on N-rGO photocatalyst for efficient degradation of 2,4-dichlorophenol. *J. Taiwan Inst. Chem. Eng.* **2018**, *93*, 603–615. [CrossRef]

35.　Yu, W.; Liu, X.; Pan, L.; Li, J.; Liu, J.; Zhang, J.; Li, P.; Chen, C.; Sun, Z. Enhanced visible light photocatalytic degradation of methylene blue by F-doped TiO$_2$. *Appl. Surf. Sci.* **2014**, *319*, 107–112. [CrossRef]

36.　Xu, J.; Ao, Y.; Fu, D.; Yuan, C. Low-temperature preparation of F-doped TiO$_2$ film and its photocatalytic activity under solar light. *Appl. Surf. Sci.* **2008**, *254*, 3033–3038. [CrossRef]

37.　Yu, C.; Fan, Q.; Xie, Y.; Chen, J.; Shu, Q.; Jimmy, C.Y. Sonochemical Fabrication of Novel Square-Shaped F Doped TiO$_2$ Nanocrystals with Enhanced Performance in Photocatalytic Degradation of Phenol. *J. Hazard. Mater.* **2012**, *237–238*, 38–45. [CrossRef]

38.　Yu, J.C.; Yu, J.; Ho, W.; Jiang, Z.; Zhang, L. Effects of F-Doping on the Photocatalytic Activity and Microstructures of Nanocrystalline TiO$_2$ Powders. *Chem. Mater.* **2002**, *14*, 3808–3816. [CrossRef]

39.　Li, X.; Zhu, J.; Li, H. Influence of crystal facets and F-modification on the photocatalytic performance of anatase TiO$_2$. *Catal. Commun.* **2012**, *24*, 20–24. [CrossRef]

40.　Li, X.; Zhang, H.; Zheng, X.; Yin, Z.; Wei, L. Visible light responsive N-F-codoped TiO$_2$ photocatalysts for the degradation of 4-chlorophenol. *J. Environ. Sci.* **2011**, *23*, 1919–1924. [CrossRef]

41.　Bao, R.; Chen, C.; Xia, J.; Chen, H.; Li, H. Controlled synthesis and enhanced photoelectro-catalytic activity of a 3D TiO$_2$ nanotube array/TiO$_2$ nanoparticle heterojunction using a combined dielectrophoresis/sol–gel method. *J. Mater. Chem. C* **2019**, *7*, 4981–4987. [CrossRef]

42.　Negi, S.S. Enhanced light harvesting and charge separation over wormhole mesoporous TiO$_{2-X}$ nanocrystallites towards efficient hydrogen generation. *Sustain. Energy Fuels* **2019**, *3*, 1191–1200. [CrossRef]

43.　Wei, N.; Liu, Y.; Feng, M.; Li, Z.; Chen, S.; Zheng, Y.; Wang, D. Controllable TiO$_2$ core-shell phase heterojunction for efficient photoelectrochemical water splitting under solar light. *Appl. Catal. B* **2019**, *244*, 519–528. [CrossRef]

44.　Zhou, J.K.; Lv, L.; Yu, J.; Li, H.L.; Guo, P.-Z.; Sun, H.; Zhao, X.S. Synthesis of Self-Organized Polycrystalline F-doped TiO$_2$ Hollow Microspheres and Their Photocatalytic Activity under Visible Light. *J. Phys. Chem. C* **2008**, *112*, 5316–5321. [CrossRef]